Transverse Magnetization in Spin-Orbit Coupled Antiferromagnets

Taekoo Oh, Sungjoon Park, and Bohm-Jung Yang*
Department of Physics and Astronomy, Seoul National University, Seoul 08826, Korea;
Center for Correlated Electron Systems, Institute for Basic Science (IBS), Seoul 08826, Korea;
and Center for Theoretical Physics (CTP), Seoul National University, Seoul 08826, Korea

(Received 15 September 2022; accepted 7 June 2023; published 29 June 2023)

Some antiferromagnets under a magnetic field develop magnetization perpendicular to the field as well as more conventional ones parallel to the field. So far, the transverse magnetization (TM) has been attributed to either the spin canting effect or the presence of cluster magnetic multipolar ordering. However, a general theory of TM based on microscopic understanding is still missing. Here, we construct a general microscopic theory of TM in antiferromagnets with cluster magnetic multipolar ordering by considering classical spin Hamiltonians with spin anisotropy that arises from the spin-orbit coupling. First, from general symmetry analysis, we show that TM can appear only when all crystalline symmetries are broken other than the antiunitary mirror, antiunitary twofold rotation, and inversion symmetries. Moreover, by analyzing spin Hamiltonians, we show that TM always appears when the degenerate ground state manifold of the spin Hamiltonian is discrete, as long as it is not prohibited by symmetry. On the other hand, when the degenerate ground state manifold is continuous, TM generally does not appear except when the magnetic field direction and the spin configuration satisfy specific geometric conditions under single-ion anisotropy. Finally, we show that TM can induce the anomalous planar Hall effect, a unique transport phenomenon that can be used to probe multipolar antiferromagnetic structures. We believe that our theory provides a useful guideline for understanding the anomalous magnetic responses of the antiferromagnets with complex magnetic structures.

DOI: 10.1103/PhysRevLett.130.266703

Introduction.—Spin-orbit coupled antiferromagnets are a promising playground to study novel correlated topological states and anomalous transport phenomena [1,2]. The complex spin structures of spin-orbit coupled antiferromagnets are characterized by their cluster magnetic multipole (CMM) reflecting the symmetry of the magnetic ground state [3,4]. Especially, those with higher-rank CMMs exhibit anomalous transport phenomena including various types of anomalous Hall effects [3–16]. The distinct magnetic symmetry of higher-rank CMMs underlies their unconventional physics, unexpected in simple spin systems with magnetic dipoles only.

Normally, when a magnetic field $\mathbf{B}$ is applied to an antiferromagnet, the magnetization develops along $\mathbf{B}$. However, transverse magnetization (TM) is also observed in anisotropic antiferromagnets including $Gd_2Ti_2O_7$, $CsMnBr_3$, and $Eu_2Ir_2O_7$ [17–22]. In $Gd_2Ti_2O_7$ and $CsMnBr_3$, TM was observed when $\mathbf{B}$ was along certain directions and was attributed to the spin canting. More recently, TM was also observed in $Eu_2Ir_2O_7$ where the magnetic octupolar ordering, not the spin canting, was proposed as the origin of TM using phenomenological theory, and the resultant TM was dubbed the orthogonal magnetization (OM) [21]. Common features of these three systems are that the antiferromagnetic ground state has higher-rank CMMs and the relevant spin Hamiltonian has spin anisotropy arising from spin-orbit coupling. Thus, to understand the fundamental origin of TM, the relation between the spin anisotropy and the complex magnetic structure with higher-rank CMMs should be clarified.

In this Letter, we construct a general microscopic theory of TM. First, through symmetry analysis, we derive the general symmetry condition to have TM. Explicitly, we show that TM emerges only when every crystalline symmetry is broken, except for twofold antiunitary rotation C_2T, antiunitary mirror σT, and inversion P. Here, C_2, σ, T indicate twofold rotation, mirror, and time-reversal symmetries, respectively. Based on the symmetry, we tabulate the information about whether TM is allowed or not under various field directions for all possible antiferromagnetic structures relevant to Mn_3Ir, $CsMnBr_3$, and pyrochlore systems including $Gd_2Ti_2O_7$ and $Eu_2Ir_2O_7$.

We also examine the microscopic origin of TM by studying the classical spin Hamiltonian on the pyrochlore lattice with spin anisotropy represented by single-ion anisotropy (SIA), Dzyaloshinskii-Moriya interaction (DMI), and dipolar interaction (DI). Depending on the nature of spin anisotropy, the antiferromagnetic ground state has distinct CMMs, and the degenerate ground state manifold (DGSM) is either discrete or continuous under spin rotation. We find that when the DGSM is discrete, TM always appears unless forbidden by symmetry. On the other

 © 2023 American Physical Society

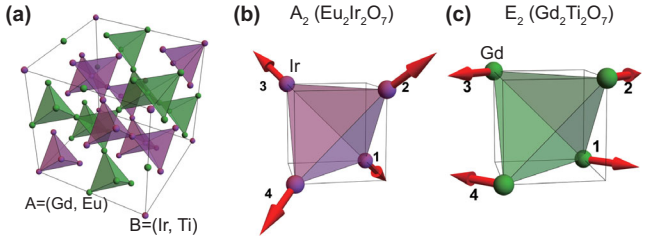

FIG. 1. (a) Structure of the pyrochlore lattice relevant to $Gd_2Ti_2O_7$ and $Eu_2Ir_2O_7$. (b),(c) Spin configurations of (b) the A_2 octupole in $Eu_2Ir_2O_7$ and (c) E_2 dotriacontapole in $Gd_2Ti_2O_7$.

hand, when DGSM is continuous, TM is generally not allowed. However, when DGSM is constrained in easy planes by SIA, TM can appear when the magnetic field direction and spin configuration satisfy certain geometric conditions. As a result of TM, we show that TM induces a unique transport phenomenon called the anomalous planar Hall effect (APHE) [23]. Although we focus on the pyrochlore lattice, our theory can be readily generalized to any antiferromagnets on any lattice system.

Global symmetry constraints.—Let us first consider the symmetry constraint on the TM ($\mathbf{M}_\perp$) under $\mathbf{B}$. First, any n-fold rotation symmetry C_n ($n = 2, 3, 4, 6$) along the direction of $\mathbf{B}$ prohibits TM because $\mathbf{M}_\perp$ is canceled by its rotated counterparts $\sum_{i=1}^{n-1} C_n^i \mathbf{M}_\perp$. Similarly, a mirror symmetry σ with the normal direction parallel to $\mathbf{B}$ forbids TM. The only unitary symmetry compatible with TM is spatial inversion P.

In the case of antiunitary symmetries, there are two symmetries compatible with $\mathbf{M}_\perp \neq 0$. One is C_2T, whose rotation axis is perpendicular to $\mathbf{B}$. In this case, $\mathbf{M}_\perp$ appears perpendicular to both the $\mathbf{B}$ and C_2 axis. The other is σT whose mirror plane is parallel to $\mathbf{B}$. Then, $\mathbf{M}_\perp$ appears on the mirror plane. As the combination of C_2T and σT is P, $\mathbf{M}_\perp$ emerges even when both symmetries exist simultaneously. In summary, every symmetry except for C_2T, σT, and P must be broken for $\mathbf{M}_\perp \neq 0$.

Using this symmetry condition, one can judge whether $\mathbf{M}_\perp$ is forbidden or not in any antiferromagnetic (AFM) system under various field directions. In the pyrochlore lattice with a tetrahedral magnetic unit cell, shown in Fig. 1, the AFM structures can be classified by group theory. The resulting irreducible representations (IRREPs) can be described in terms of CMMs [3,4] including the A_2 octupole ($\hat{A}_2$), T_1 octupoles ($\hat{T}_{1x}, \hat{T}_{1y}, \hat{T}_{1z}$), T_2 octupoles ($\hat{T}_{2x}, \hat{T}_{2y}, \hat{T}_{2z}$), and E dotriacontapoles ($\hat{E}_1, \hat{E}_2$) [3,4,21,24–28]. In the case of $\hat{A}_2$, shown in Fig. 1, for example, its magnetic point group $-4'3m'$ contains an identity I, three twofold rotations C_2, eight threefold rotations C_3', six antiunitary mirrors σT, and six fourfold antiunitary inversion S_4T. For $\mathbf{B}\|[001]$, every symmetry, except I, C_{2z}, and two σTs, is broken. Because there is C_{2z}, $\mathbf{M}_\perp = 0$. On the other hand, when $\mathbf{B}\|[110]$, only I and a σT remain, thus $\mathbf{M}_\perp$ can be nonzero. We extend this analysis to the D_{3h} point group relevant to $CsMnBr_3$ [17] and to the O_h point group relevant to Mn_3Ir [3,16,29–32] [see Supplemental Material (SM) [33]].

The analysis of the magnetic point group under $\mathbf{B}$ determines the direction of $\mathbf{M}_\perp$ and its general $\mathbf{B}$ dependence. For instance, let us consider an AFM ordering with the magnetic point group $\mathbb{P}$, which is described by the Hamiltonian $H(\{\mathbf{S}_a\})$ where a indicates the lattice site. When $\mathbf{B}$ is applied, most symmetries in $\mathbb{P}$ are broken but they strongly constrain the spin canting directions. More explicitly, for an element $O_p \in \mathbb{P}$, we have

$$U(O_p)H(\{\mathbf{S}_a\}, \mathbf{B})U(O_p)^{-1} = H(\{\mathbf{S}_a\}, \mathbf{B}_p), \quad (1)$$

where $\mathbf{B}_p = O_p\mathbf{B}$ and $U(O_p)$ is the matrix representation of O_p. Namely, O_p effectively changes the direction of $\mathbf{B}$ while keeping the spin structure. For example, let us recall $\hat{A}_2$ under $\mathbf{B}\|[110]$. Among the symmetries in $\mathbb{P}$, $\mathbb{P}_1 = \{I, \sigma_{[1\bar{1}0]}T\}$ indicates the symmetry that leaves $\mathbf{B}$ invariant. Here I denotes the identity and $\sigma_{[1\bar{1}0]}$ is the mirror symmetry with $[1\bar{1}0]$ normal vector. On the other hand, $\mathbb{P}_2 = \{C_{2z}, \sigma_{[110]}T\}$ denotes the symmetries which invert the direction of $\mathbf{B}$. Here $\sigma_{[110]}$ is the mirror symmetry with [110] normal vector. Applying $\mathbb{P}_1$ and $\mathbb{P}_2$ symmetries to the constraint equation in Eq. (1), we obtain $\mathbf{M}_\perp \propto [bB^2 + O(B^4)]\hat{z}$ with a constant b. A similar analysis can also be applied to other CMMs. In the case of $\hat{E}_2$ under $\mathbf{B}\|[111]$, we find that $\mathbb{P}_1 = \{I\}$ leaves $\mathbf{B}$ invariant while $\mathbb{P}_2 = \{\sigma_{[1\bar{1}0]}\}$ inverts the $\mathbf{B}$ direction, which gives $\mathbf{M}_\perp = (bB^2 + \ldots)\hat{e}_{1\bar{1}0} + (dB + fB^3 + \ldots)\hat{e}_{11\bar{2}}$ where b, d, f are constants. Detailed $\mathbf{B}$ dependence of TM is determined by microscopic spin interactions as discussed below. The cases of E_1 and T_{2y} CMMs under $\mathbf{B}\|[111]$ are analyzed in the SM.

Microscopic Hamiltonian.—The classical Heisenberg antiferromagnet on the pyrochlore lattice has macroscopically degenerate ground states [43,44]. Under $\mathbf{B}$, the Hamiltonian becomes

$$\begin{aligned} H_0 = H_J + H_B &= J\sum_{\langle ab\rangle} \mathbf{S}_a \cdot \mathbf{S}_b - \sum_a \mathbf{B}\cdot\mathbf{S}_a, \\ &= 8JN_c\mathbf{M}^2 - 4N_c\mathbf{B}\cdot\mathbf{M} - \frac{JN_c}{2}\sum_{a=1}^{4}\mathbf{S}_a^2, \end{aligned} \quad (2)$$

where H_J with $J > 0$ indicates the isotropic antiferromagnetic exchange between nearest-neighboring spins, and H_B is the Zeeman coupling. N_c is the number of tetrahedral unit cells, $\mathbf{M} = \frac{1}{4}\sum_{a=1}^{4}\mathbf{S}_a$ is the average magnetization of the four spins in a tetrahedron. From $\mathbf{S}_a^2 = 1$, we obtain $H_0 = 8JN_c[\mathbf{M} - (\mathbf{B}/4J)]^2$. Then, the minimum energy condition gives $\mathbf{M} = (\mathbf{B}/4J)$. Namely, TM vanishes when spin anisotropy is absent.

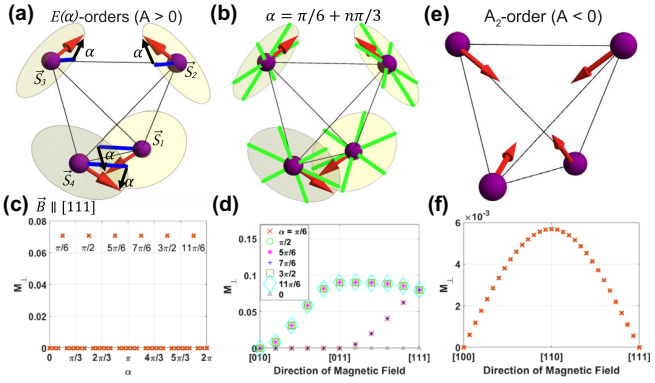

FIG. 2. (a) $\hat{E}(\alpha)$ order when $A > 0$. The spins (red arrows) are lying on their easy planes (yellow planes). (b) Green lines denote the spin directions of $\hat{E}(\pi/6 + n\pi/3)$ orders $(n = 0, \ldots, 5)$. (c) $\mathbf{M}_\perp$ for $\hat{E}(\alpha)$ order as a function of α when $\mathbf{B}\|[111]$. $\mathbf{M}_\perp \neq 0$ only at $\alpha = \pi/6 + n\pi/3$. (d) $\mathbf{M}_\perp$ for $\hat{E}(\alpha)$ order with various α computed by changing $\mathbf{B}$ from [010] to [011], and to [111]. (e) $\hat{A}_2$ order when $A < 0$. (f) $\mathbf{M}_\perp$ for $\hat{A}_2$ order computed by changing $\mathbf{B}$ from [100] to [110], and to [111]. In (c),(d),(f), we choose $|A|/J = B/J = 1$.

Single-ion anisotropy (SIA).—Let us consider $H_1 \equiv H_0 + H_{\mathrm{SIA}}$ that includes $H_{\mathrm{SIA}} = A\sum_a (\mathbf{S}_a \cdot \mathbf{n}_a)^2$. When $A > 0$, H_{SIA} forces $\mathbf{S}_a$ to lie on its easy plane: $\mathbf{S}_a \cdot \mathbf{n}_a = 0$ [see Fig. 2(a)]. The energy minimum condition of H_1 is

$$\mathbf{M} = \frac{\mathbf{B}}{4J}, \qquad \mathbf{S}_a \cdot \mathbf{n}_a = 0 (a = 1, 2, 3, 4). \tag{3}$$

When $\mathbf{B} = 0$, the ground state is antiferromagnetic with either the E dotriacontapole or T_2 octupole, in which all spins are lying on their easy planes. As the E dotriacontapole belongs to a two-dimensional (2D) IRREP, it is composed of two basis states, the $\hat{E}_1$ and $\hat{E}_2$ orders. Similarly, the T_2 octupole belonging to a three-dimensional (3D) IRREP is composed of three basis states, the $\hat{T}_{2x}$, $\hat{T}_{2y}$, and $\hat{T}_{2z}$ orders (see SM).

Specifically, in the $\hat{E}_1$ order, the four spins $\mathbf{S}_{a=1,2,3,4}$ in a unit cell are aligned along the directions $\hat{x}_1 = [1\bar{1}0]$, $\hat{x}_2 = [110]$, $\hat{x}_3 = [\bar{1}\,\bar{1}\,0]$, $\hat{x}_4 = [\bar{1}10]$, respectively, while for the $\hat{E}_2$ order, the spins are along $\hat{y}_1 = [11\bar{2}]$, $\hat{y}_2 = [1\bar{1}2]$, $\hat{y}_3 = [\bar{1}12]$, $\hat{y}_4 = [\bar{1}\,\bar{1}\,\bar{2}]$, respectively. Then, a general E dotriacontapole is represented by $\hat{E}(\alpha) = \hat{E}_1 \sin\alpha + \hat{E}_2 \cos\alpha$, which spans a continuous DGSM parametrized by $0 \leq \alpha \leq 2\pi$ [see Fig. 2(a)]. As α varies, the spins continuously rotate on their easy planes. Similar to $[\hat{E}_1, \hat{E}_2]$ orders, $[\hat{E}(\alpha = \pi/6), \hat{T}_{2x}]$ orders, $[\hat{E}(\alpha = 5\pi/6), \hat{T}_{2y}]$ orders, and $[\hat{E}(\alpha = \pi/2), \hat{T}_{2z}]$ orders form pairs of basis states which span continuous DGSM where spins are lying on their easy planes.

When $\mathbf{B} \neq 0$, the energy minimum condition in Eq. (3) is satisfied in most cases, thus TM vanishes. But there are some exceptional cases with nonzero TM. For example, for a given $\hat{E}(\alpha)$ order at $\mathbf{B} = 0$, the spin configuration at small $\mathbf{B}$ can be parametrized as

$$\mathbf{S}_a = \cos\theta_a[\cos(\alpha + \phi_a)\hat{x}_a + \sin(\alpha + \phi_a)\hat{y}_a] - \sin\theta_a \hat{z}_a, \tag{4}$$

where ϕ_a (θ_a) indicates the rotation within (away from) the easy plane of $\mathbf{S}_a$ because of $\mathbf{B} \neq 0$. At small $\mathbf{B}$, we expand $\mathbf{S}_a$ up to the first order of (θ_a, ϕ_a) and put it in Eq. (3), which gives $\mathbf{S}_a \cdot \mathbf{n}_a = -\theta_a = 0$, $M_x = (1/4\sqrt{6})[(\cos\alpha - \sqrt{3}\sin\alpha) \times (\phi_1 + \phi_2 - \phi_3 - \phi_4)]$, $M_y = (1/4\sqrt{6})[(\cos\alpha + \sqrt{3}\sin\alpha)(\phi_1 - \phi_2 + \phi_3 - \phi_4)]$, $M_z = (-1/2\sqrt{6})[\cos\alpha(\phi_1 - \phi_2 - \phi_3 + \phi_4)]$. Note that when $\tan\alpha = 1/\sqrt{3}$, $M_x = 0$. Then, $M_x = B_x/(4J)$ in Eq. (3) cannot be satisfied if $B_x \neq 0$. Similar situations occur when $\tan\alpha = -1/\sqrt{3}$ and $B_y \neq 0$, or $\cos\alpha = 0$ and $B_z \neq 0$.

Interestingly, these are exactly the conditions to have nonzero TM [see Fig. 2(b)]. For instance, for the $\hat{E}(\alpha = \pi/6, 7\pi/6)$ order with $\tan\alpha = 1/\sqrt{3}$, when $\mathbf{B}\|[100]$, the projection of $\mathbf{B}$ onto the easy plane of each spin is parallel to the corresponding spin direction, thus $\mathbf{B}$ cannot rotate each spin within its easy plane. Instead, $\mathbf{B}$ forces the spins to move away from their easy planes, violating Eq. (3) and inducing nonzero TM. Similar situations happen for $\hat{E}(5\pi/6, 11\pi/6)$ order with $B_y \neq 0$, and $\hat{E}(\pi/2, 3\pi/2)$ order with $B_z \neq 0$.

The spin configuration with nonzero TM can be obtained by the stationary condition $\partial H_1/\partial\theta_a = \partial H_1/\partial\phi_a = 0$. For instance, for $\hat{E}(\pi/2)$ order under $\mathbf{B}\|[111]$ described in Fig. 2(b), the stationary condition gives $\theta_1 = \theta_4 = -\theta_2 = -\theta_3 = [B/(6A + 4J)]$, $\phi_1 = \phi_4 = 0$, $\phi_2 = -\phi_3 = -(B/\sqrt{6}J)$, from which we obtain $\mathbf{M}_\perp = [\sqrt{2}/4(2 + 3A/J)] \times (A/J)(B/J)\hat{e}_{11\bar{2}}$. As $\theta_{1,2,3,4}$ are nonzero, all spins move away from their easy planes. In Fig. 2(c), we compute $\mathbf{M}_\perp$ for $\hat{E}(\alpha)$ order under $\mathbf{B}\|[111]$ varying α. In Fig. 2(d), we plot $\mathbf{M}_\perp$ for various $\hat{E}(\alpha)$ orders by continuously rotating $\mathbf{B}$ from [010] to [011], and then to [111] in sequence. $\mathbf{M}_\perp$ becomes nonzero only when the special conditions between $\mathbf{B}$ and α described above are satisfied (see SM for further discussions).

When $A < 0$, on the other hand, each spin $\mathbf{S}_a$ aligns along its easy-axis direction $\mathbf{n}_a$, leading to the all-in-all-out ground state with an A_2 octupole shown in Fig. 2(e). Two degenerate ground states, the all-in or all-out state, related by time-reversal symmetry form a discrete manifold in which the states are separated by an energy barrier, contrary to the $A > 0$ case. In this situation, we find that TM generally appears unless it is forbidden by symmetry. We compute TM by changing $\mathbf{B}$ from [010] to [101], and then to [111] continuously, and represent the result in Fig. 2(f). Considering symmetry, TM vanishes for $\mathbf{B}\|[001]$ and [111]. For other directions, TM is nonzero and exhibits $|\mathbf{M}_\perp| \propto (A/J)(B/J)^2$ consistent with magnetic space

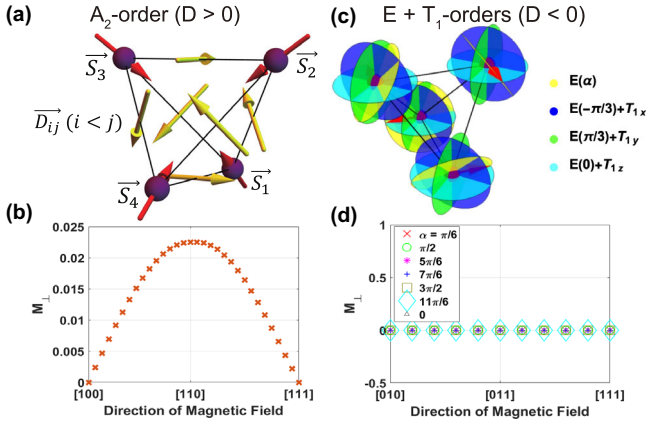

FIG. 3. (a) $\hat{A}_2$ order when $D > 0$, where all spins (red arrows) are perpendicular to the surrounding DM vectors (yellow arrows). (b) $\mathbf{M}_\perp$ for $\hat{A}_2$ order computed by changing $\mathbf{B}$ from [100] to [110] and to [111]. (c) Schematic description of continuous DGSM when $D < 0$. There are four distinct planes; yellow planes are for $\hat{E}(\alpha)$ order, blue planes are for $\hat{E}(-\pi/3) + \hat{T}_{1x}$ order, green planes are for $\hat{E}(\pi/3) + \hat{T}_{1y}$ order, and cyan planes are for $\hat{E}(0) + \hat{T}_{1z}$ order. (d) $\mathbf{M}_\perp$ for $\hat{E}(\alpha)$ order with various α computed by changing $\mathbf{B}$ from [010] to [011] and to [111]. In (b),(d), we assume $|D|/J = B/J = 1$.

group analysis. All these results are further confirmed by numerically solving H_1 (see SM).

Dzyaloshinskii-Moriya interaction (DMI).—Next, we consider $H_2 \equiv H_0 + H_{\rm DMI}$ that includes $H_{\rm DMI} = D\sum_{\langle ab\rangle} \hat{\mathbf{D}}_{ab} \cdot (\mathbf{S}_a \times \mathbf{S}_b)$. Generally, DMI forces two spins $\mathbf{S}_a$ and $\mathbf{S}_b$ to lie in their planes perpendicular to the DM vector $\hat{\mathbf{D}}_{ab}$ so that $\mathbf{S}_a \times \mathbf{S}_b$ is antiparallel (parallel) to $\hat{\mathbf{D}}_{ab}$ when $D > 0$ ($D < 0$).

Let us first consider the $D > 0$ case [27]. In the pyrochlore lattice, DMI forces each spin to be perpendicular to its six neighboring DM vectors, and the intersection between the planes normal to those DM vectors is uniquely determined, which leads to the $\hat{A}_2$ order as shown in Fig. 3(a). As in the case of SIA with $A < 0$, since DGSM is discrete, TM generally arises unless prohibited by symmetry. For example, in Fig. 3(b), we compute the TM by changing $\mathbf{B}$ from [100] to [110], and then to [111]. When $\mathbf{B}\|[100]$ and [111], TM vanishes because of rotation symmetries. Otherwise, TM is nonzero. From the stationary condition of H_2, we obtain $|\mathbf{M}_\perp| \propto (D/J)(B/J)^2$ (see SM for more details).

On the other hand, when $D < 0$, the relative angle between neighboring spins is inverted compared to the $D > 0$ case to minimize the energy. To find the ground state for $D < 0$, we rewrite H_2 by adding some constants as

$$H_2 = -12D\left(\sum_a \mathbf{S}_a \cdot \hat{v}_a/4\right)^2 - 8D\sum_{r=1}^{3}\left[\left(\sum_a \mathbf{S}_a \cdot \mathbf{T}_a^r/4\right)^2\right] + 8(J - D/2)\left(\mathbf{M} - \frac{\mathbf{B}}{4(J - D/2)}\right)^2, \quad (5)$$

where $\hat{v}_a$ is the unit vector along the local z axis of $\mathbf{S}_a$, and $\mathbf{T}_a^r$ ($r = 1, 2, 3$) indicates the spin direction relevant to the T_2 octupole. The explicit forms of $\hat{v}_a$ and $\mathbf{T}_a^r$ are given in the SM. Since $D < 0$, all coefficients of squared terms in H_2 are positive, thus H_2 can be minimized when the following seven equations are satisfied:

$$\mathbf{M} = \frac{\mathbf{B}}{4J - 2D}, \quad \sum_{a=1}^{4} \mathbf{S}_a \cdot \hat{v}_a = 0, \quad \sum_{a=1}^{4} \mathbf{S}_a \cdot \mathbf{T}_a^r = 0. \quad (6)$$

When $\mathbf{B} = 0$, one can show that $[\hat{E}_1, \hat{E}_2]$ orders span the continuous DGSM as in the case of SIA with $A > 0$. Similarly, $[\hat{E}(\alpha = 0), \hat{T}_{1z}]$ orders, $[\hat{E}(\alpha = \pi/3), \hat{T}_{1y}]$ orders, and $[\hat{E}(\alpha = -\pi/3), \hat{T}_{1x}]$ orders form pairs of basis states which span continuous DGSM where spins are lying on the xy, zx, and yz planes, respectively [see Fig. 3(c)].

Since DGSM is continuous, one can generally expect TM to vanish. To check possible exceptional situations as in the SIA case with $A > 0$, let us consider $\hat{E}(\alpha)$ order at $\mathbf{B} = 0$ and examine the spin configuration at small $\mathbf{B}$ by introducing angular variation (θ_a, ϕ_a) as in Eq. (4). Plugging the parametrized form of spins in Eq. (4) into Eq. (6), we obtain, up to the linear order in $B = |\mathbf{B}|$, $\theta_a = -3\hat{z}_a \cdot [\mathbf{B}/4(J - D/2)]$, $\phi_a = q[B/4(J - D/2)]$ where q is an arbitrary constant. Contrary to the SIA case with $A > 0$ in which $\theta_a = 0$ is always required to minimize the SIA term irrespective of $\mathbf{B}$, here, both θ_a and ϕ_a can continuously vary under $\mathbf{B}$ while the energy minimum condition is satisfied. As spins can rotate continuously in three-dimensional space under $\mathbf{B}$ while satisfying Eq. (6), TM vanishes. This is generally true for arbitrary $\hat{E}(\alpha)$ under arbitrary $\mathbf{B}$, as shown in Fig. 3(d). The same results can be obtained from the stationary conditions $\partial H_2/\partial\theta_a = \partial H_2/\partial\phi_a = 0$. All these results can be further confirmed by numerical calculation of H_2 (see SM). Other $\hat{E} + \hat{T}_1$-type ground states with continuous DGSM exhibit similar behaviors as discussed in the SM.

Similar relations also hold in systems with dipolar interactions as shown in the SM.

Anomalous planar Hall effect (APHE).—In metallic antiferromagnets with CMMs, TM can induce APHE [23], i.e., simultaneous appearance of the anomalous Hall effect (AHE) and planar Hall effect (PHE) [34,45,46]. This is because an applied in-plane $\mathbf{B}$ generates both in-plane $\mathbf{M}_{\perp,\rm in}$ and out-of-plane $\mathbf{M}_{\perp,\rm out}$ TM, which give PHE and AHE, respectively [see Fig. 4(a)].

Motivated by the recent observation of AHE and PHE in pyrochlore iridates [22,25], we examine APHE in this system with $\hat{A}_2$ order. Assuming $\hat{x}\|[1\bar{1}0]$, $\hat{y}\|[11\bar{2}]$, and $\hat{z}\|[111]$, we apply an electric field $\mathbf{E}\|\hat{x}$, and rotate $\mathbf{B}$ within the $\hat{x}\,\hat{y}$ plane. Considering the symmetry of the pyrochlore lattice, we find $M_{\perp,\rm out} = (a_0 + a_1\cos 3\theta + b_1 \sin 3\theta)\hat{z}$, $M_{\perp,\rm in} = (c_1 \cos 3\theta)\hat{p}$ where a_0, a_1, b_1, and c_1 are constants, and $\hat{p} = (-\sin\theta, \cos\theta, 0)$ is the in-plane unit vector

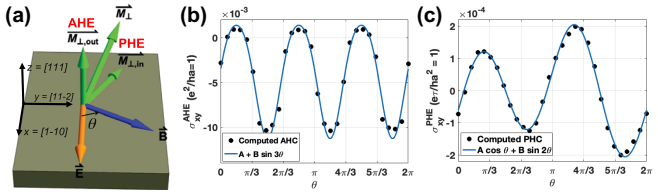

FIG. 4. (a) Schematic description of TM and APHE. (b) The computed AHC (black dots) and its fitting (blue line) by $\beta_0 + \beta_2 \sin 3\theta$. (c) The computed PHC (black dots) and its fitting (blue line) by $\gamma_1 \cos\theta + \delta_1 \sin 2\theta$.

perpendicular to $\mathbf{B}$ [see Fig. 4(a)]. Using the phenomenological model for anomalous Hall conductivity (AHC) and planar Hall conductivity (PHC) [35,47] given by $\sigma_{xy}^{\mathrm{AHE}} = \sigma_0 M_{\perp,\mathrm{out}}$, $\sigma_{xy}^{\mathrm{PHE}} = \sigma_1 B_x B_y + \sigma_2 (B_x M_{\perp,y} + B_y M_{\perp,x}) + \sigma_3 M_{\perp,x} M_{\perp,y}$, we obtain

$$\begin{aligned} \sigma_{xy}^{\mathrm{AHE}} &\propto \beta_0 + \beta_1 \cos 3\theta + \beta_2 \sin 3\theta, \\ \sigma_{xy}^{\mathrm{PHE}} &\propto \gamma_1 \cos\theta + \gamma_2 \cos 5\theta \\ &\quad + \delta_1 \sin 2\theta + \delta_2 \sin 4\theta + \delta_3 \sin 8\theta, \end{aligned} \tag{7}$$

where $\beta_{0,1,2}$, $\gamma_{1,2}$, and $\delta_{1,2,3}$ are constants. γ_1, γ_2 terms come from the σ_2 term while δ_1, δ_2, δ_3 come from the σ_3 term in $\sigma_{xy}^{\mathrm{PHE}}$.

To confirm the prediction of the phenomenological theory, we perform self-consistent mean-field calculations of the Hubbard model describing pyrochlore iridates with $\hat{A}_2$ order [24,36], and numerically compute the AHC [37] and PHC [34] (see SM for details). For AHC, we consider only the intrinsic Berry curvature contribution while for PHC, we assume constant relaxation time. The resulting AHC (PHC) is plotted using black dots in Fig. 4(b) [Fig. 4(c)] which can be fitted by $\sigma_{xy}^{\mathrm{AHE}} \propto \beta_0 + \beta_2 \sin 3\theta$ and $\sigma_{xy}^{\mathrm{PHE}} \propto \gamma_1 \cos\theta + \delta_1 \sin 2\theta$, respectively, consistent with Eq. (7). Note that experimental data can contain additional terms due to rare-earth ions and strain, etc. [22]. As APHE probes multipolar AFM structures through its relation with TM, it can be further applied to the systems where conventional methods like neutron scattering do not work [18–20].

Discussion.—Our theory can explain the experiments on $CsMnBr_3$, $Gd_2Ti_2O_7$, $Eu_2Ir_2O_7$ which are well described by classical spin Hamiltonians because of the large spin in $Gd_2Ir_2O_7$ ($S = 7/2$) and $CsMnBr_3$ ($S = 5/2$), and stable AFM ordering in $Eu_2Ir_2O_7$ [27]. First, in $CsMnBr_3$, $\mathbf{M}_\perp \propto B$ is observed when $\mathbf{B}$ is in the xz plane unless $\mathbf{B} \| \hat{x}, \hat{z}$ [17]. When $\mathbf{B} \| \hat{x}(\hat{z})$, $\sigma_x(\sigma_z, C_{3z})$ forbids TM. When $\mathbf{B}$ is in the xz plane, C_{2y}, which inverts $\mathbf{B}$, enforces $\mathbf{M}_\perp \propto B$. In $Gd_2Ir_2O_7$, $\mathbf{M}_\perp = 0$ for $\mathbf{B} \| [001], [110]$ and $\mathbf{M}_\perp \neq 0$ for $\mathbf{B} \| [111], [112]$ were observed [18–20]. For $\mathbf{B} \| [001]([110])$, $C_{2z}(\sigma_{[110]})$ forbids TM. For other $\mathbf{B}$, as all symmetries are broken, TM appears. Finally, in $Eu_2Ir_2O_7$, $\mathbf{M}_\perp \propto B^2 \sin 2\theta$ was observed [21]. When $\mathbf{B} \| \hat{x}, \hat{y}$, twofold rotation forbids TM, whereas when $\mathbf{B}$ is within the xy plane, $S_4 T$, which inverts $\mathbf{B}$, enforces $\mathbf{M}_\perp \propto B^2$. S_4 denotes fourfold improper rotation. Thus, $\mathbf{M}_\perp \propto B^2 \sin 2\theta$. All these experiments are consistent with our symmetry analysis and numerical results (see SM).

Considering that TM was also observed in fluctuating spin models [48], we believe that understanding the influence of quantum fluctuations on TM is one important direction for future study.

T. O., S. P., and B.-J. Y. were supported by the Institute for Basic Science in Korea (Grant No. IBS-R009-D1), Samsung Science and Technology Foundation under Project No. SSTF-BA2002-06, and the National Research Foundation of Korea (NRF) grant funded by the Korea government (MSIT) (No. 2021R1A2C4002773 and No. NRF-2021R1A5A1032996).

*bjyang@snu.ac.kr

[1] Y. Tokura, K. Yasuda, and A. Tsukazaki, Nat. Rev. Phys. **1**, 126 (2019).
[2] W. Witczak-Krempa, G. Chen, Y. B. Kim, and L. Balents, Annu. Rev. Condens. Matter Phys. **5**, 57 (2014).
[3] M.-T. Suzuki, T. Koretsune, M. Ochi, and R. Arita, Phys. Rev. B **95**, 094406 (2017).
[4] M.-T. Suzuki, T. Nomoto, R. Arita, Y. Yanagi, S. Hayami, and H. Kusunose, Phys. Rev. B **99**, 174407 (2019).
[5] L. Šmejkal, R. González-Hernández, T. Jungwirth, and J. Sinova, Sci. Adv. **6**, eaaz8809 (2020).
[6] Y. Gao and D. Xiao, Phys. Rev. B **98**, 060402(R) (2018).
[7] R. Matsumoto, R. Shindou, and S. Murakami, Phys. Rev. B **89**, 054420 (2014).
[8] E. G. Mishchenko and O. A. Starykh, Phys. Rev. B **90**, 035114 (2014).
[9] V. A. Zyuzin and A. A. Kovalev, Phys. Rev. Lett. **117**, 217203 (2016).
[10] R. Cheng, S. Okamoto, and D. Xiao, Phys. Rev. Lett. **117**, 217202 (2016).
[11] S. Park, N. Nagaosa, and B.-J. Yang, Nano Lett. **20**, 2741 (2020).
[12] W. J. Kim, J. H. Gruenewald, T. Oh, S. Cheon, B. Kim, O. B. Korneta, H. Cho, D. Lee, Y. Kim, M. Kim *et al.*, Phys. Rev. B **98**, 125103 (2018).
[13] K. Ueda, T. Oh, B.-J. Yang, R. Kaneko, J. Fujioka, N. Nagaosa, and Y. Tokura, Nat. Commun. **8**, 15515 (2017).
[14] K. Ueda, R. Kaneko, H. Ishizuka, J. Fujioka, N. Nagaosa, and Y. Tokura, Nat. Commun. **9**, 3032 (2018).
[15] T. Ohtsuki, Z. Tian, A. Endo, M. Halim, S. Katsumoto, Y. Kohama, K. Kindo, M. Lippmaa, and S. Nakatsuji, Proc. Natl. Acad. Sci. U.S.A. **116**, 8803 (2019).
[16] Y. Zhang, J. Železný, Y. Sun, J. Van Den Brink, and B. Yan, New J. Phys. **20**, 073028 (2018).
[17] S. Abarzhi, A. Bazhan, L. Prozorova, and I. Zaliznyak, J. Phys. Condens. Matter **4**, 3307 (1992).
[18] V. N. Glazkov, M. E. Zhitomirsky, A. I. Smirnov, H.-A. Krug von Nidda, A. Loidl, C. Marin, and J.-P. Sanchez, Phys. Rev. B **72**, 020409(R) (2005).
[19] V. Glazkov, C. Marin, and J. Sanchez, J. Phys. Condens. Matter **18**, L429 (2006).

[20] V. Glazkov, M. Zhitomirsky, A. Smirnov, C. Marin, J. Sanchez, A. Forget, D. Colson, and P. Bonville, J. Phys. Condens. Matter **19**, 145271 (2007).
[21] T. Liang, T. H. Hsieh, J. J. Ishikawa, S. Nakatsuji, L. Fu, and N. Ong, Nat. Phys. **13**, 599 (2017).
[22] Y. Li, T. Oh, J. Son, J. Song, M. K. Kim, D. Song, S. Kim, S. H. Chang, C. Kim, B.-J. Yang *et al.*, Adv. Mater. **33**, 2008528 (2021).
[23] R. Battilomo, N. Scopigno, and C. Ortix, Phys. Rev. Res. **3**, L012006 (2021).
[24] T. Oh, H. Ishizuka, and B.-J. Yang, Phys. Rev. B **98**, 144409 (2018).
[25] W. J. Kim, T. Oh, J. Song, E. K. Ko, Y. Li, J. Mun, B. Kim, J. Son, Z. Yang, Y. Kohama *et al.*, Sci. Adv. **6**, eabb1539 (2020).
[26] S. E. Palmer and J. T. Chalker, Phys. Rev. B **62**, 488 (2000).
[27] M. Elhajal, B. Canals, R. Sunyer, and C. Lacroix, Phys. Rev. B **71**, 094420 (2005).
[28] M. J. Gingras and P. A. McClarty, Rep. Prog. Phys. **77**, 056501 (2014).
[29] Y. Zhang, Y. Sun, H. Yang, J. Železný, S. P. P. Parkin, C. Felser, and B. Yan, Phys. Rev. B **95**, 075128 (2017).
[30] I. Tomeno, H. N. Fuke, H. Iwasaki, M. Sahashi, and Y. Tsunoda, J. Appl. Phys. **86**, 3853 (1999).
[31] J. M. Taylor, E. Lesne, A. Markou, F. K. Dejene, B. Ernst, A. Kalache, K. G. Rana, N. Kumar, P. Werner, C. Felser *et al.*, Phys. Rev. Mater. **3**, 074409 (2019).
[32] H. Chen, Q. Niu, and A. H. MacDonald, Phys. Rev. Lett. **112**, 017205 (2014).
[33] See Supplemental Material at http://link.aps.org/supplemental/10.1103/PhysRevLett.130.266703 for details which includes Refs. [3,17–19,21,24,26,27,34–42].
[34] S. Nandy, G. Sharma, A. Taraphder, and S. Tewari, Phys. Rev. Lett. **119**, 176804 (2017).
[35] Y. Wang, P. A. Lee, D. Silevitch, F. Gomez, S. Cooper, Y. Ren, J.-Q. Yan, D. Mandrus, T. Rosenbaum, and Y. Feng, Nat. Commun. **11**, 216 (2020).
[36] W. Witczak-Krempa, A. Go, and Y. B. Kim, Phys. Rev. B **87**, 155101 (2013).
[37] N. Nagaosa, J. Sinova, S. Onoda, A. H. MacDonald, and N. P. Ong, Rev. Mod. Phys. **82**, 1539 (2010).
[38] F. Seitz, Phys. Rev. **79**, 372 (1950).
[39] A. B. Pippard, *Magnetoresistance in Metals* (Cambridge University Press, Cambridge, England, 1989), Vol. 2.
[40] J. Stewart, G. Ehlers, A. Wills, S. T. Bramwell, and J. Gardner, J. Phys. Condens. Matter **16**, L321 (2004).
[41] G. B. Sim and S. B. Lee, Phys. Rev. B **98**, 014423 (2018).
[42] A. Chubukov, J. Phys. C **21**, L441 (1988).
[43] J. S. Gardner, M. J. B. Gingras, and J. E. Greedan, Rev. Mod. Phys. **82**, 53 (2010).
[44] R. Moessner and J. T. Chalker, Phys. Rev. Lett. **80**, 2929 (1998).
[45] S.-H. Zheng, H.-J. Duan, J.-K. Wang, J.-Y. Li, M.-X. Deng, and R.-Q. Wang, Phys. Rev. B **101**, 041408(R) (2020).
[46] V.-D. Ky, Sov. Phys. JETP **23**, 809 (1966), http://www.jetp.ras.ru/cgi-bin/dn/e_023_05_0809.pdf.
[47] S. Nandy, A. Taraphder, and S. Tewari, Sci. Rep. **8**, 14983 (2018).
[48] B. Irsigler, J.-H. Zheng, M. Hafez-Torbati, and W. Hofstetter, Phys. Rev. A **99**, 043628 (2019).